Available online at www.sciencedirect.com
ScienceDirect
Journal of Pharmaceutical and Biomedical Analysis 43 (2007) 1195–1205
JOURNAL OF PHARMACEUTICAL AND BIOMEDICAL ANALYSIS
www.elsevier.com/locate/jpba

Metabolism of a $^{14}C/^{3}H$-labeled $GABA_A$ receptor partial agonist in rat, dog and human liver microsomes: Evaluation of a dual-radiolabel strategy

Christopher L. Shaffer*, Connie S. Langer

Department of Pharmacokinetics, Pharmacodynamics and Metabolism, Pfizer Global Research and Development, Groton/New London Laboratories, Pfizer Inc., Groton, CT 06340, USA

Received 25 September 2006; received in revised form 15 November 2006; accepted 17 November 2006
Available online 5 December 2006

Abstract

The metabolism of 2-{[2-(3-fluoropyrid-2-yl)-1*H*-imidazol-1-yl]methyl}-1-propyl-5-cyano-1*H*-benzimidazole (**1**), a potent subtype-selective $GABA_A$ receptor partial agonist, was investigated in rat, dog and human liver microsomes. Due to its significant metabolic cleavage at C_8 observed in preliminary biotransformation studies with non-radiolabeled **1**, both [^{14}C]**1** and [^{3}H]**1** were synthesized with respective radioisotopes placed on either side of C_8 to determine if all microsomal metabolites formed after C_8 *N*-dealkylation of **1** (or its core-intact metabolites) could be detected and quantified adequately. Both radiolabeled forms of **1**, used separately in mono-radiolabel studies in cross-species microsomes and concomitantly in dual-radiolabel studies in rat microsomes, permitted the detection and quantification of all metabolites of **1**, and a combination of radioactive and mass spectral data allowed structural elucidation of its Phase I metabolites. As expected, the sum of ^{14}C-only metabolites equaled that of ^{3}H-only metabolites in all incubations. In-line radiometric analysis worked extremely well (and was very reproducible) for quantifying either ^{14}C- or ^{3}H-compounds within *separate* incubations when using mono-radiolabeled **1**. However, although the in-line radiodetector provided a comprehensive *qualitative* metabolic profile using dual-radiolabled **1**, its inability to exclude completely ^{14}C- from ^{3}H-generated counts caused a degree of ambiguity pertaining to metabolite quantification. Thus, off-line liquid scintillation counting of collected dual-radiolabeled incubation LC-fractions was employed to *quantify* both ^{14}C- and ^{3}H-metabolites simultaneously, while in-line radiodetection was only used for *qualitative* analyses accompanying MS and MS/MS experiments. These studies demonstrated the analytical feasibility of using a dual-radiolabel approach for subsequent in vivo ADME studies with **1**.

Keywords: In vitro drug metabolism; Dual-radiolabel compounds; Metabolite structure elucidation

1. Introduction

Deciphering metabolic pathways in both preclinical species and humans is critical in the evaluation of a new chemical entity (NCE) [1–4]. Initial studies in drug discovery typically assess NCE stability in human hepatic in vitro systems since the liver is most often the prime organ of metabolic importance for xenobiotics [5]. These studies attempt to identify metabolically susceptible sites within the NCE potentially amenable to synthetic modification for improved metabolic stability resulting in superior pharmacology and safety. Prior to clinical trials, the in vitro metabolic profile of an NCE is determined in hepatic tissue systems of the proposed toxicological species and humans to provide a preliminary idea of the appropriateness of such species from a drug metabolism perspective. Because such initial studies typically employ a non-radiolabeled NCE and lack authentic standards of yet to be determined metabolites, they purely afford qualitative and (at best) semi-quantitative metabolite information for only those metabolites detectable by non-radioactive techniques (e.g. UV and/or MS). Due to these analytical shortcomings, as well as in vitro systems often being only partially telling of in vivo clearance mechanisms, radiolabeled NCE is administered to toxicological species and humans during compound development for the definitive determination of excretory and metabolic pathways to ensure that human metabolites are adequately evaluated in toxicology studies [6,7]. Radioactivity

* Corresponding author. Tel.: +1 860 441 3377; fax: +1 860 686 6532.
E-mail address: Christopher.L.Shaffer@pfizer.com (C.L. Shaffer).

0731-7085/$ – see front matter © 2006 Elsevier B.V. All rights reserved.
doi:10.1016/j.jpba.2006.11.022

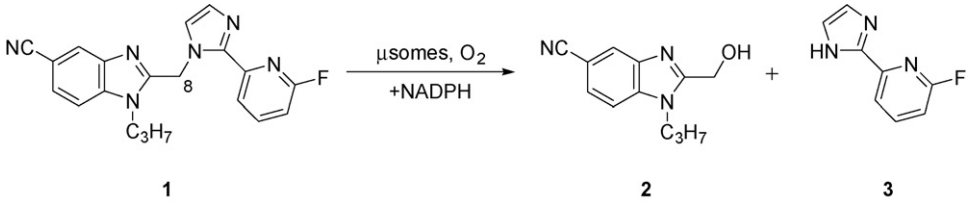

Fig. 1. The NADPH-dependent microsomal-mediated metabolic scission of **1** into **2** and **3**.

allows direct detection and quantification of metabolites irrespective of intrinsic molecular properties that dictate their detection by the currently preferred analytical techniques of liquid chromatography–tandem mass spectrometry (LC–MS/MS) [8–11] or traditional HPLC with UV detection [12,13].

Compound **1**, a potent subtype-selective partial agonist at the $GABA_A$ receptor complex, significantly reduces in rats both spontaneous locomotor activity and the latency to assume a sleep posture without the well-known side effects of commonly available hypnotics [14–16]. Initial in vitro biotransformation studies using non-radiolabeled **1** in cross-species hepatic microsomes suggested it underwent significant metabolic scission to benzimidazole alcohol **2** and fluoropyridine imidazole **3** in an NADPH-dependent manner (Fig. 1). Due to the availability of authentic standards **2** and **3**, their metabolic stability was assessed similarly to determine if either underwent further metabolism; in the presence of NADPH, **2** was inert while **3** was extensively metabolized. Hence, prior to the initiation of in vivo biotransformation studies with a radiolabeled form of **1**, both [^{14}C]**1** and [^{3}H]**1** (Fig. 2) were synthesized with respective radioisotopes placed on either side of C_8, the site of metabolic fragmentation, to determine if all microsomal metabolites formed after C_8 *N*-dealkylation of **1** (or its core-intact metabolites) could be detected adequately. Compound **1** was radiolabeled with different isotopes so that a mixture of the two radioisoforms could be monitored simultaneously without the confusion of changes in specific activity of mono-radiolabeled metabolites that might occur using **1** dually labeled with the same radioisotope. Both radiolabeled forms of **1**, used separately in mono-radiolabeled studies in cross-species microsomes and concomitantly in dual-radiolabeled studies in rat microsomes, permitted the detection and quantification of all metabolites of **1**. A combination of radioactive and mass spectral data allowed elucidation of the Phase I metabolic pathways of **1** in rat, dog and human liver microsomes.

2. Experimental

2.1. Chemicals and reagents

Compounds **1**–**3** were provided by Neurogen Corporation (Branford, CT); [^{14}C]**1** (49.9 mCi/mmol, 99.7% radiochemical purity) and [^{3}H]**1** (23.7 Ci/mmol, 99.5% radiochemical purity) were synthesized by the Radiochemical Synthesis Group at Pfizer Global Research and Development (PGRD, Ann Arbor, MI). The chemical purity of all synthetic compounds was >99%. Male Sprague–Dawley rat liver microsomes (RLMs; 21.0 mg protein/mL, 0.61 nmol P450/mg protein), male beagle dog liver microsomes (DLMs; 18.6 mg protein/mL, 0.36 nmol P450/mg protein) and human liver microsomes (HLMs, a pool of 45 donor livers; 19.5 mg protein/mL, 0.32 nmol P450/mg protein) were prepared, characterized and stored at −70 °C prior to use by the Candidate Enhancement Group at PGRD (Groton, CT). Chemicals and solvents of reagent or HPLC grade were supplied by Aldrich Fine Chemical Co. (Milwaukee, WI), Fisher Scientific (Pittsburgh, PA) and the J. T. Baker Chemical Co. (Phillipsburg, NJ). TruCount liquid scintillation cocktail was purchased from IN/US Systems, Inc. (Tampa, FL).

2.2. Microsomal incubations

Hepatic microsomes were thawed on wet ice just prior to use. Incubations (3 mL) were performed in duplicate with and without NADPH (3.9 μmol) in round-bottom glass test tubes open to air at 37 °C in a shaking water bath. Each incubation contained, in order of addition, 2385 μL of KH_2PO_4 buffer (pH 7.4; 0.1 M), 300 μL of RLMs, DLMs or HLMs (ca. 2 mg protein/mL), 15 μL of a 2 mM substrate (**1**–**3**) stock solution dissolved in acetonitrile (yielding an initial incubation substrate concentration of 10 μM), and 300 μL of a 13 mM NADPH solution containing 33 mM $MgCl_2$. For incubations with [^{14}C]**1** or [^{3}H]**1**, radiolabeled material was diluted with non-radiolabeled **1** to

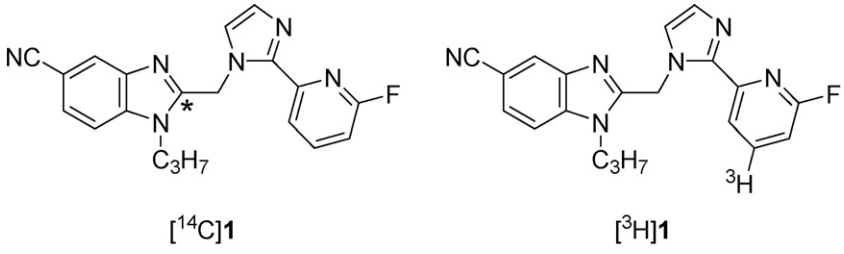

Fig. 2. Chemical structures for [^{14}C]**1** (symbol '*' denotes ^{14}C) and [^{3}H]**1**.

provide 10 μM incubations with either 0.25 μCi of [^{14}C]**1** or 2.5 μCi of [^{3}H]**1** for mono-radiolabeled studies, or 0.25 μCi of [^{14}C]**1** and 2.5 μCi of [^{3}H]**1** for dual-radiolabeled studies. Sample aliquots (1 mL) were removed from incubations after NADPH (or $MgCl_2$) addition by micropipette at 0, 30 and 60 min for mono-radiolabeled studies, and at 0 and 60 min for dual-radiolabeled studies. Aliquots were quenched with acetonitrile (5 mL), precipitated microsomal proteins were sedimented by centrifugation (1811 rcf for 10 min), and the resulting supernatant was concentrated under N_2 at 40 °C and reconstituted in 1 mL of acetonitrile–ammonium formate (pH 3.5; 10 mM) (15:85, v/v).

2.3. Radioactivity recovery analyses

At each step during the preparation of analytical samples from radioactive incubations, total radioactivity levels were determined by liquid scintillation counting (LSC) for recovery calculations to determine the extent (if any) of radioactive binding to microsomal proteins and/or formation of volatile metabolites. Aliquots (10 μL), taken from the unquenched incubation sample aliquot (1 mL), from the supernatant following centrifugation of the quenched sample aliquot (ca. 6 mL), and from the reconstituted analytical sample (1 mL) after supernatant concentration, were removed by micropipette, mixed with liquid scintillation cocktail (7 mL) and analyzed for 5 min by a Wallac 1409 DSC liquid scintillation counter (Perkin-Elmer Life and Analytical Sciences, Inc., Wellesley, MA). Scintillation counter data were automatically corrected for ^{14}C or ^{3}H counting efficiency using an external standardization technique and an instrument-stored quench curve generated from a series of sealed quench standards. For samples containing ^{14}C and ^{3}H, a dual-radiolabeled LSC program was used which corrected for energy overlaps following customary procedures.

Although the tritium atom within [^{3}H]**1** was predicted to be resistant to chemical- and metabolism-mediated loss, incubations with [^{3}H]**1** were nonetheless analyzed for tritiated water (HTO), the molecular reporter of ^{3}H-loss. The following procedure was undertaken to quantify both total radioactivity and HTO within a mono-radiolabeled tritiated incubation with microsomes from each species: a gravimetric aliquot (1 g) from an unquenched incubation at each time point (i.e. 0, 30 and 60 min) was transferred to a borosilicate glass tube (12 mm × 75 mm, Pyrex®) immersed in wet ice. Duplicate gravimetric aliquots (0.25 g) were mixed with scintillation cocktail (7 mL) and counted for 5 min by LSC as described previously. Subsequently, each glass tube containing the remaining sample (0.5 g) was capped with a Kimwipe® secured by a rubber band, frozen at −20 °C and lyophilized using a FreeZone 4.5 Benchtop Freeze Dry System (Labconco Corporation, Kansas City, MO). Each lyophilized sample was reconstituted in H_2O (2.5 g) and vortex-mixed, and duplicate gravimetric aliquots (0.5 g) were combined with scintillation cocktail (7 mL) and counted for 5 min by LSC. Additionally, each Kimwipe® was submerged in scintillation cocktail (7 mL) and analyzed for radioactivity via LSC. The difference in total radioactivity within each incubation sample before and after lyophilization was attributed to HTO. Scintillation counter data were automatically corrected for ^{3}H counting efficiency as described previously.

2.4. LC–MS/MS sample analysis with radiometric detection

Samples were analyzed by an LC–MS/MS, comprised of a PE Sciex API-3000 tandem quadrupole mass spectrometer with a Turbo Ionspray interface (Perkin-Elmer Life and Analytical Sciences, Boston, MA), two Shimadzu LC-10A HPLC pumps (Shimadzu USA, Columbia, MD) and a CTC PAL Autosampler (LEAP Technologies, Carrboro, NC), in series with a β-RAM radiometric detector (IN/US Systems, Inc.) containing a liquid scintillant cell (500 μL). Analytes within sample aliquots (50–100 μL) were eluted on a Phenomenex C_{18} analytical column (5 μm, 150 mm × 4.6 mm) at 0.6 mL/min with ammonium formate (pH 3.5; 10 mM) (Solvent A) and acetonitrile (Solvent B). The binary gradient was programmed as follows: 0–12 min, 15% Solvent B in Solvent A; 12–47 min, 15–40% B in A; 47–57 min, 40–90% B in A. Following elution of **1** and its metabolites, the column was washed with 90% B in A for 3 min and then returned over 3 min to 15% B in A where it remained for 8 min prior to the next injection. For all radioactive samples, >95% of the radioactivity injected onto the column eluted during the first 57 min of the gradient program. HPLC effluent was split 1:9 between the mass spectrometer and the radiometric flow detector; liquid scintillation cocktail flowed at 3 mL/min to the radiometric detector. Mass spectral data were collected using positive ionization in full, precursor ion, neutral loss, product ion and multiple-reaction monitoring (MRM) scanning modes. The source temperature was 350 °C, and the nebulizer and auxiliary gas pressures were 8.0 A.U. For MS/MS experiments, the collisionally activated decomposition gas pressure was 4.0 A.U. and the collision energy was −30 eV. However, instrument operation modes, settings and potentials were adjusted accordingly to provide optimal data for specific experiments. Analyst® 1.4 (Perkin-Elmer Life and Analytical Sciences) and Winflow Version 1.5(3) (IN/US Systems, Inc.) software were used for the acquisition and processing of mass spectral and radiochromatographic data, respectively. Metabolites were quantified by peak integration within generated radiochromatograms.

For dual-radiolabeled samples, a unique dual-channel method was created to monitor ^{3}H and ^{14}C simultaneously by the β-RAM detector. Energy windows were adjusted to measure from 0 to 2 V in Channel 1 for ^{3}H detection and from 2 to 10 V in Channel 2 for ^{14}C detection, resulting in efficiencies of 30 and 50% for ^{3}H and ^{14}C, respectively, with a compensation for ^{14}C spill-over into the ^{3}H channel of 38%. The latter was determined by injection of mono-radiolabeled standards. For comparison, LC effluent from separate injections of the same dual-radiolabeled samples was isolated in 30 s intervals by a Gilson FC 204 fraction collector (Gilson, Inc., Middleton, WI), and each fraction (ca. 270 μL) was mixed with liquid scintillation cocktail (7 mL) and analyzed by the dual-radiolabeled LSC program already described. Radiochromatograms generated by in-line and off-line radiometric detection were then compared qualitatively and quantitatively.

2.5. LC–MS/MS sample analysis with UV detection

Authentic standards **2** and **3**, the direct C_8 *N*-dealkylation products of **1**, were incubated in RLMs to determine their metabolic fates. Since **2** and **3** were not radiolabeled, incubation aliquots were analyzed using the same LC–MS/MS methods described beforehand, but each compound was quantified by MS using MRM scanning mode following *m/z* 216.1 → 156.1 fragmentation for **2**, and *m/z* 164.3 → 110.2 transition for **3**. In an attempt to detect metabolites (if any) of **2** and **3**, LC effluent was monitored by single wavelength UV detection using an in-line Spectro Monitor 3200 variable wavelength detector (Thermo Electron Corporation, Waltham, MA), with the selection of analytical wavelengths determined by the respective UV–vis spectrum of each standard. Stock solutions (23 μM) of **2** and **3** in acetonitrile–water (pH 3.0) (3:7, v/v) were analyzed by a Shimadzu UV-2101 PC UV–vis scanning spectrophotometer (Shimadzu USA, Columbia, MD) from 200–500 nm in a 1 cm crystal cell. For **2**, $\lambda_{max} = 218$ nm ($\varepsilon_{218} = 52{,}449\ cm^{-1}\ M^{-1}$, $\varepsilon_{254} = 7169\ cm^{-1}\ M^{-1}$), and for **3** $\lambda_{max} = 289$ nm ($\varepsilon_{289} = 18{,}733\ cm^{-1}\ M^{-1}$, $\varepsilon_{300} = 16{,}187\ cm^{-1}\ M^{-1}$). Thus, **2** and **3** incubation samples were monitored at analytical wavelengths of 254 and 300 nm, respectively; different analytical wavelengths were also used in an attempt to distinguish compound-dependent metabolites simultaneously.

3. Results and discussion

3.1. Mono-radiolabel incubations with [^{14}C]1 and [^{3}H]1

Incubations with either [^{14}C]**1** or [^{3}H]**1** were conducted in duplicate in RLMs, DLMs and HLMs for 30 and 60 min in both the absence and presence of NADPH. In all studies, 95–106% of the initial radioactivity was extracted from the microsomal protein, ≤3% of the extracted radioactivity was lost upon supernatant concentration and >97% of the radioactivity detected in the radiochromatogram was identified as either **1** or a unique metabolite. In incubations lacking NADPH, no new radioactive peaks were generated over time suggesting **1** underwent neither NADPH-independent biotransformation nor chemical degradation. Furthermore, in all incubations (±NADPH) the amount of radioactivity detected from 0 to 60 min remained unchanged, signifying volatile metabolites were not generated and **1** did not evaporate from the microsomal suspension. For all tritiated incubations, 96–103% of the radioactivity present prior to lyophilization was detected afterwards indicating no formation of HTO during the microsomal consumption of [^{3}H]**1** confirming the chemical and metabolic stability of its tritium atom.

For quantitative metabolite profiling within mono-radiolabeled microsomal incubations, [^{14}C]**1** and [^{3}H]**1** were first assessed individually to determine the percent contribution of each metabolite to total radioactivity within respective radiochromatograms (e.g. Table 1 and Fig. 3 for RLMs, 60 min). Metabolites within ^{14}C- or ^{3}H-radiochromatograms retained the benzimidazole or fluoropyridine of **1**, respectively. The overall contribution of a metabolite to the biotransformation

Table 1
Quantitative in-line-generated profile of [^{14}C]metabolites, [^{3}H]metabolites and total metabolites after a 60 min mono-radiolabeled incubation with either [^{14}C]**1** or [^{3}H]**1** in rat liver microsomes

Compound	[^{14}C]**1**	[^{3}H]**1**	Average
1	3.9	1.6	2.8
M1	–	3.8	1.9
3	–	41.6	20.8
M3	–	7.9	4.0
M4	–	1.7	0.9
M5	–	9.0	4.5
M6	3.3	2.7	3.0
M7	5.2	3.2	4.2
M8	7.9	4.4	6.2
M9	2.9	2.0	2.5
M10	–	1.4	0.7
2	55.7	–	27.9
M12	–	–	–
M13	4.0	–	2.0
M15	5.8	3.9	4.9
M16	–	3.2	1.6
M17	6.1	7.8	7.0
M18	–	2.0	1.0
M19	–	–	–
M20	–	1.1	0.6
M21	–	–	–
M22	5.1	3.1	4.1
Radioactivity profiled (%)	99.9	100.4	100.2
Σ^{3}H-only metabolites (**M1**, **3**, **M3**–**M5**)	na	64.0	32.0
Σ^{14}C-only metabolites (**2**, **M13**, **M19**)	59.7	na	29.9

–, not detected by radiochromatography; na, not applicable.

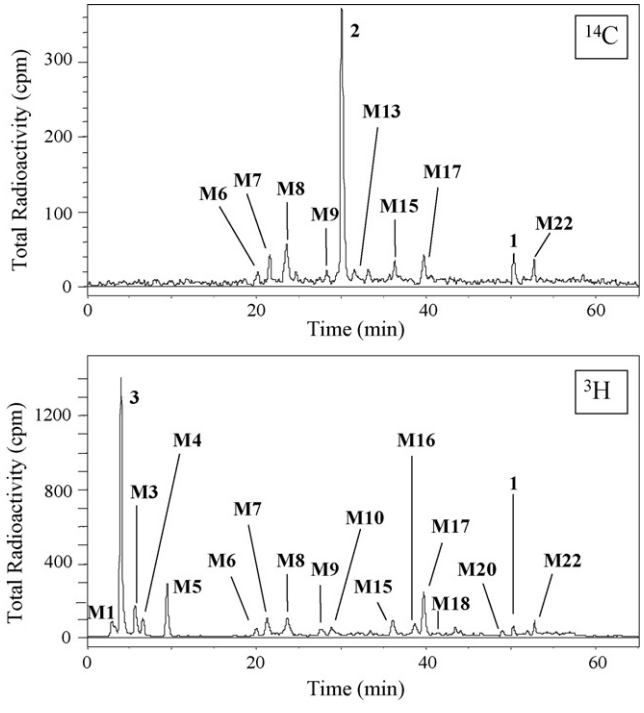

Fig. 3. In-line radiochromatograms of mono-radiolabeled incubations in rat liver microsomes with [^{14}C]**1** (top) or [^{3}H]**1** (bottom) after 60 min.

Table 2
Quantitative in-line-generated profile of mean metabolites of **1** after 30 and 60 min mono-radiolabeled incubations with either [^{14}C]**1** or [^{3}H]**1** in cross-species liver microsomes

Compound	30 min			60 min		
	Rat	Dog	Human	Rat	Dog	Human
1	7.8	66.9	73.1	2.8	51.5	58.2
M1	1.5	0.8	0.1	1.9	1.3	0.2
3	20.4	2.3	1.5	20.8	2.2	1.8
M3	2.5	1.0	0.8	4.0	1.8	0.9
M4	1.6	0.3	0.4	0.9	0.3	0.5
M5	4.5	6.7	5.9	4.5	7.4	7.7
M6	–	–	–	3.0	–	–
M7	3.7	–	–	4.2	0.4	–
M8	4.0	–	–	6.2	–	–
M9	2.2	2.0	1.5	2.5	3.1	2.7
M10	1.7	–	–	0.7	0.6	–
2	29.1	4.6	2.5	27.9	6.1	3.8
M12	–	–	–	–	–	–
M13	–	–	–	2.0	–	–
M15	3.0	1.2	2.6	4.9	2.5	4.8
M16	2.6	0.5	–	1.6	1.5	–
M17	7.3	1.5	3.0	7.0	2.4	4.4
M18	2.4	1.9	–	1.0	2.9	–
M19	–	4.3	5.3	–	6.6	9.0
M20	1.5	5.2	0.9	0.6	8.1	0.7
M21	–	0.4	0.6	–	0.9	1.5
M22	2.6	0.5	1.4	4.1	0.9	2.6
Radioactivity profiled (%)	98.4	99.7	99.3	100.2	100.0	98.6
Σ^{3}H-only metabolites (**M1**, **3**, **M3**–**M5**)	30.5	11.0	8.7	32.0	12.9	11.0
Σ^{14}C-only metabolites (**2**, **M13**, **M19**)	29.1	8.9	7.8	29.9	12.7	12.8

–, not detected by radiochromatography.

of **1** was calculated by averaging the mono-radiolabel data. Derived from this procedure, a quantitative summary of the metabolites observed in cross-species hepatic microsomes containing both NADPH and either [^{14}C]**1** or [^{3}H]**1** after 30 and 60 min of incubation is found in Table 2.

3.1.1. Rat liver microsomes

After 30 and 60 min of [^{14}C]**1** incubation in RLMs, 6.8 and 3.9% of **1** remained, respectively, and 7 and 9 (all 30 min metabolites + **M6** and **M13**) new peaks were detected radiometrically (Fig. 3, Tables 1 and 2). After 30 and 60 min of [^{3}H]**1** incubation in RLMs, 8.8 and 1.6% of **1** remained, respectively, and 15 and 16 (all 30 min metabolites + **M6**) new peaks were observed by radiodetection (Fig. 3, Tables 1 and 2). In RLMs, essentially complete NADPH-dependent oxidation of **1** occurred within 30 min, and the major route of metabolism (ca. 30% of overall consumption of **1**) was C_8 *N*-dealkylation of **1** and/or its core-intact metabolites to **2** and **3** (Table 3).

Although [^{3}H]**1** was more useful than [^{14}C]**1** in determining the overall metabolic fate of **1** in RLMs, it alone did not reveal the *entire* metabolic picture since it did not permit radiometric detection of ^{14}C-only metabolites **2** and **M13** (Fig. 3). A similar shortcoming was found for [^{14}C]**1** regarding the radiometric compensation of ^{3}H-only metabolites **M1**, **3**, and **M3**–**M5**. Importantly, the percent of total radioactivity comprised by ^{14}C-only metabolites (29.9%) equaled that of ^{3}H-only metabolites (32.0%).

3.1.2. Dog liver microsomes

After 30 and 60 min of [^{14}C]**1** incubation in DLMs, 69.5 and 52.5% of **1** remained, respectively, and 7 (**M9**, **2**, **M15** and **M17**–**M20**) and 9 (all 30 min peaks + **M7** and **M16**) metabolites were detected radiometrically. After 30 and 60 min of [^{3}H]**1** incubation in DLMs, 64.3 and 50.4% of **1** remained, respectively, and 13 (**M1**, **3**, **M3**–**M5**, **M9**, **M15**–**M18** and **M20**–**M22**) and 15 (all 30 min peaks + **M10** and **M19**) metabolites were observed by radiodetection (Table 2). In DLMs, biotransformation of **1** was NADPH-dependent, and the major (≥10% of net metabolism of **1**) routes of metabolism after 60 min were formation of **M5**, **2**, **M19** and **M20** (Table 3).

The data suggest that RLMs and DLMs generate similar metabolites, but DLMs metabolize **1** to a much lesser extent (and at a much slower rate). Additionally, biotransformation of **1** after 60 min into ^{14}C-only (12.7%) and ^{3}H-only (12.9%) metabolites is only one of four significant metabolic pathways in DLMs, and the extent of this cleavage is essentially unchanged between 30 and 60 min of incubation (Tables 2 and 3).

3.1.3. Human liver microsomes

After 30 and 60 min of [^{14}C]**1** incubation in HLMs, 75.3 and 57.7% of **1** remained, respectively, and 6 (**2**, **M15**, **M17**, **M19**, **M21** and **M22**) and 7 (30 min peaks + **M9**) metabolites were detected radiometrically. After 30 and 60 min of [^{3}H]**1** incubation in HLMs, 70.9 and 58.7% of **1** remained, respectively, and the same 12 (**M1**, **3**, **M3**–**M5**, **M9**, **M15**, **M17** and

Table 3
Cross-species summary of each metabolite as a percentage of the net metabolism of **1** after 60 min in hepatic microsomes containing NADPH

Compound	Rat[a]		Dog[a]	Human[a]
	Mono-label[b]	Dual-label[c]	Mono-label[b]	Mono-label[b]
M1	2.0	0.7	2.7	0.5
3	21.4	20.1	4.4	4.3
M3	4.1	–	3.6	2.0
M4	0.9	2.6	0.5	1.2
M5	4.6	9.0	15.2	18.3
M6	3.1	0.7	–	–
M7	4.3	2.8	0.7	–
M8	6.3	5.9	–	–
M9	2.5	2.8	6.4	6.5
M10	0.7	–	1.1	–
2	28.6	24.7	12.5	9.1
M12	–	1.6	–	–
M13	2.1	–	–	–
M15	5.0	4.5	5.1	11.5
M16	1.6	1.2	3.1	–
M17	7.1	6.7	4.8	10.5
M18	1.0	3.5	5.9	–
M19	–	1.5	13.6	21.5
M20	0.6	–	16.6	1.6
M21	–	–	1.9	3.5
M22	4.2	–	1.9	6.2

–: not detected by radiochromatography.
[a] Values are reported as percentages of net metabolism. A specific value determined for a metabolite (e.g. **MX**) is determined from 60 min mono- or dual-radiolabel incubation data by: (% **MX**/(100-% **1** remaining)) × 100.
[b] In-line generated data.
[c] LSC-generated data.

M19–**M22**) metabolites were observed after both 30 and 60 min of incubation (Table 2). The HLM metabolism of **1** was NADPH-dependent, and the major routes of its conversion after 60 min were to **M5**, **2**, **M15**, **M17** and **M19** (Table 3).

All HLM metabolites of **1** were also formed in RLMs and/or DLMs, and **1** was metabolized to a similar extent and rate in both HLMs and DLMs. Enzyme-catalyzed cleavage of **1** after 60 min into ^{14}C-only (12.8%) and ^{3}H-only (11.0%) metabolites, which was similar after 30 or 60 min of incubation, occurred to a similar degree as in DLMs, and is only one of five significant metabolic pathways in HLMs (Table 3). Although not as critical in HLMs (or DLMs) as in RLMs due to the decreased amount of C_8 *N*-dealkylation, all mono-radiolabeled incubations across species validated using dual-radiolabeled **1** to provide its *entire* liver microsome-generated metabolic profile simultaneously.

3.2. Dual-radiolabel incubations with [^{14}C]1 and [^{3}H]1

For dual-radiolabel studies, the simultaneous detection of ^{14}C and ^{3}H within the same sample posed analytical challenges. The energies of β-particles emitted from ^{3}H range from 0–18.6 keV, while those from ^{14}C range from 0–155 keV [17]; mean energies of ^{3}H- and ^{14}C-derived β-particles are 5.6 and 52 keV, respectively [18,19]. Therefore, due to the overlapping nature of the ^{3}H and ^{14}C energy distribution spectra, the amount of radioactivity attributable to each isotope was determined by selectively measuring different energy ranges (i.e. "channels") for each radioisotope (i.e. 0–18.6 keV for ^{3}H and 18.6–155 keV for ^{14}C) while still completely capturing its mean energy region, which corresponds to its greatest percentage of total emissions. Since the energy spectrum of ^{14}C completely overlaps that of ^{3}H, it was impossible to distinguish fully ^{3}H-derived β-emissions from those of ^{14}C. Therefore, the amount of radioactivity deemed attributable to a ^{3}H-containing metabolite might be artificially high, since a metabolite containing both ^{3}H and ^{14}C would have total β-emissions from both radioisotopes detected within the ^{3}H energy channel. This phenomenon is generically referred to as "cross-talk." Alternatively, because the energy channel set for ^{14}C detection completely excluded ^{3}H-derived β-emissions, no cross-talk was possible in ^{14}C-radiochromatograms of dual-radiolabel incubations. However, a portion of the β-emissions arising from ^{14}C was not counted using the dual-channel method since the lower energy range of 0–18.6 keV was excluded from the ^{14}C energy channel.

With this cross-talk caveat in mind, in-line radiodetection versus LC fraction collection and LSC analysis (i.e. off-line radiodetection) was evaluated for the quantification of radioactive metabolites in dual-radiolabel studies. Although the employed in-line radiodetector was technically able to perform cross-talk subtraction calculations in real-time, which ultimately allows simultaneously normalized-^{3}H- and ^{14}C-radiodetection, these complex mathematical calculations can potentially hinder the precision of dual-radiolabel quantification even when the instrument parameters are adjusted optimally. Complicating matters further is the fact that for an in-line detector the radioactive effluent within the flow cell may not interact with the inflowing liquid scintillant for the length of time required for optimal photon generation. This would cause lower counts detected within the instrument resulting in even more ambiguity during cross-talk normalization calculations leading to unreliable quantification data. However, traditional LSC analysis of fraction collected LC samples would allow for more reliable dual-radiolabel radiodetection for a number of reasons. First, radioactive effluent would interact with the liquid scintillant for a longer period of time and be counted over a more sustained period, allowing for more accurate data. Secondly, greater confidence could be achieved in setting the ^{3}H and ^{14}C energy windows within the LSC accordingly, so that radioactivity arising from either radioisotope could be determined more reliably due to no need for complicated normalization calculations required by the in-line radiodetector. Thus, it was decided to use in-line radiodetection for the *qualitative* LC–MS single isotope analysis of samples (i.e. confirming that a specific radioisotope peak coeluted with a specific *m/z*), and LSC for the *quantitative* analysis of samples. Thus, for dual-radiolabel incubations, **1** and its metabolites were quantified by averaging the relative percent of radioactivity associated with each identified peak from sequential fraction collection and LS counting of ^{3}H and ^{14}C simultaneously using a dual-radiolabel protocol.

A mixture of [^{14}C]**1** and [^{3}H]**1** was incubated in RLMs (±NADPH) for 60 min. The dual-radiolabel approach was only tested in RLMs since mono-radiolabeled studies demonstrated RLMs afforded the most complex metabolite profile of **1**. In all

studies, ≥96% of the initial radioactivity was extracted from the microsomal protein, no radioactivity was lost upon supernatant concentration and >91% of total radioactivity detected in the radiochromatogram was identified as either **1** or a unique metabolite; no new radioactive peaks were generated over time in incubations lacking NADPH. Furthermore, in all incubations (±NADPH) the amount of radioactivity detected in each incubation from 0 to 60 min remained unchanged, and >97% of the radioactivity present prior to lyophilization was detected afterwards.

After 60 min of [^{14}C/^{3}H]**1** incubation, 25.9% of **1** remained and 15 metabolites were observed radiometrically by both in-line and off-line analyses (Figs. 4 and 5, Table 4). Metabolites **M20**, **M21** and **M22**, which were detected by both in-line radiodetection (Fig. 4) and MS, were not detected by LSC (Fig. 5) due to the loss in peak resolution upon fraction collection. Conversely, metabolites **M9**, **M12** and **M19** were detected by both LSC and MS, but not by in-line radioanalysis, due to the greater sensitivity of the LSC methodology. Although **1** was metabolized to a lesser extent by RLMs using [^{14}C/^{3}H]**1** than either mono-radiolabeled substrate, a virtually identical metabolic profile (both quantitatively and qualitatively) was observed (Fig. 3 versus Figs. 4 and 5), suggesting the dual-radiolabel analytical methodology was functioning optimally. One additional metabolite, **M12**, was detected radiometrically by LSC in the dual-radiolabel 60 min incubation. Although **M12** was not previously detected radiometrically, its protonated molecular ion was observed by LC–MS in all previous mono- and dual-radiolabel incubations containing NADPH. This suggests that **M12** is generated at quantities that fall below the lower

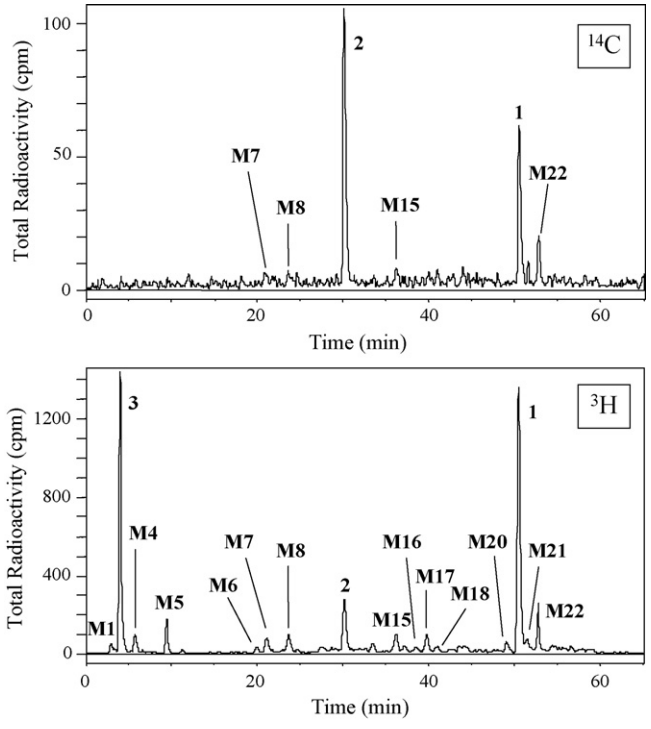

Fig. 4. In-line radiochromatograms of dual-radiolabeled incubations in rat liver microsomes with [^{14}C/^{3}H]**1** after 60 min. Top, ^{14}C channel; bottom, ^{3}H channel.

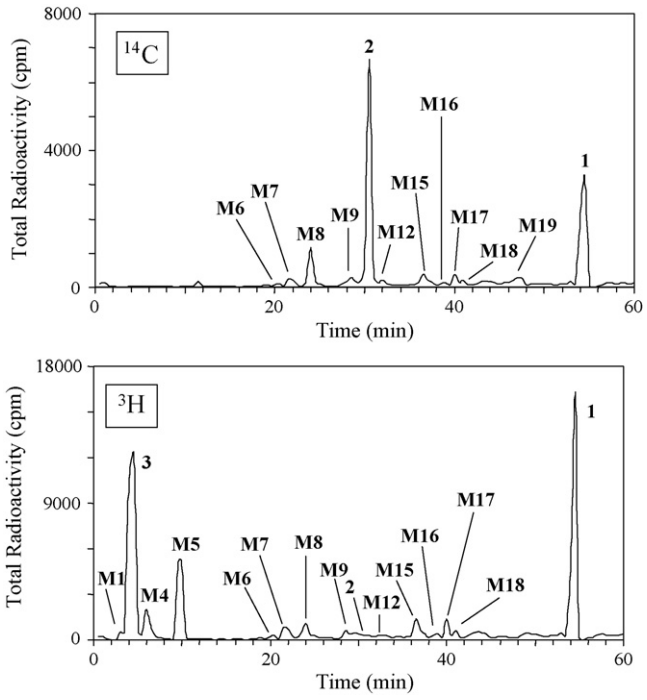

Fig. 5. LSC-generated radiochromatograms of dual-radiolabeled incubations in rat liver microsomes with [^{14}C/^{3}H]**1** after 60 min. Top, ^{14}C channel; bottom, ^{3}H channel.

Table 4
Quantitative LSC-generated profile of [^{14}C]metabolites, [^{3}H]metabolites and total metabolites after a 60 min dual-radiolabeled incubation with [^{14}C]**1** and [^{3}H]**1** in rat liver microsomes

Compound	[^{14}C]Channel	[^{3}H]Channel	Average
1	23.7	28.0	25.9
M1	–	1.0	0.5
3	–	29.8	14.9
M3	–	–	–
M4	–	3.8	1.9
M5	–	13.3	6.7
M6	0.5	0.4	0.5
M7	2.1	2.0	2.1
M8	6.5	2.2	4.4
M9	3.0	1.1	2.1
M10	–	–	–
2	36.0	0.5[a]	18.3
M12	1.8	0.6	1.2
M13	–	–	–
M15	3.7	2.9	3.3
M16	1.1	0.8	0.9
M17	6.9	3.1	5.0
M18	3.0	2.1	2.6
M19	2.2	–	1.1
M20	–	–	–
M21	–	–	–
M22	–	–	–
Radioactivity profiled (%)	90.5	91.6	91.4
Σ^{3}H-only metabolites (**M1**, **3**, **M3**–**M5**)	0.0	46.4	23.2
Σ^{14}C-only metabolites (**2**, **M13**, **M19**)	38.2	0.5[a]	19.4

–: not detected by radiochromatography.
[a] Cross-talk detected within the ^{3}H-channel from ^{14}C-only metabolite **3**.

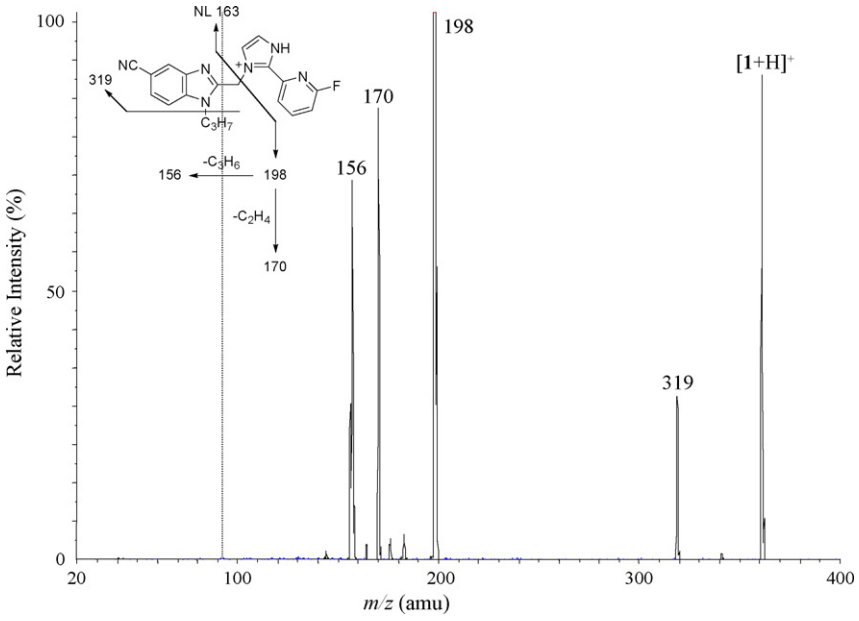

Fig. 6. Collision-induced dissociation spectrum of protonated **1** (*m/z* 361) and its proposed fragmentation pathways.

limit of detection (LLOD) for in-line radioanalysis, but above the LLOD for LSC analysis. In both instances, however, these same quantities of **M12** were well above the LLOD for MS analysis, and so **M12** was detected by MS without the detection of a corresponding radioactive peak. Lastly, three metabolites (**M3**, **M10** and **M13**) previously observed in mono-radiolabel incubations were not observed in the dual-radiolabel study most likely due to the decreased extent of metabolism of **1** resulting in no formation of these proposed downstream metabolites.

For RLMs, the use of [^{14}C/^{3}H]**1** facilitated the simultaneous radiochromatographic detection of *all* metabolites (i.e. ^{14}C-only, ^{3}H-only and ^{14}C/^{3}H-compounds) found in the prerequisite studies with mono-radiolabeled **1** (Table 3). As in mono-radiolabel studies, the dual-radiolabel studies demonstrated that after

Table 5
Chromatographic and mass spectral data for **1** and its metabolites

Compound	LC t_R (min)	$[M+H]^+$ (*m/z*)	Product ions[a] (*m/z*)	^{14}C[b]	^{3}H[b]	PC 198[c]	NL 163[c]
1	50.1	361	361, 319, **198**, 170, 156	+	+	+	+
M1	2.9	nd	na	−	+	−	−
3	4.1	164	164, 144, 137, 128, 123, **110**, 96, 83, 42	−	+	−	−
M3	5.4	nd	na	−	+	−	−
M4	6.4	nd	na	−	+	−	−
M5	9.3	nd	na	−	+	−	−
M6	19.2	nd	na	−	+	−	−
M7	21.4	nd	na	−	+	−	−
M8	23.3	287	243, 215, **198**, 170, 156, 111, 69	+	+	+	−
M9	27.3	337	320, 215, **198**, 170, 156	+	+	+	−
M10	28.5	353	336, 215, **198**, 170, 156	+	+	+	−
2	29.6	216	198, 183, 174, 170, **156**, 43	+	−	+	−
M12	30.2	377	319, 214, 196, **170**, 164	+	+	−	+
M13	31.4	286	241, **198**, 170, 156	+	−	+	−
M15	36.1	377	335, **198**, 170, 156	+	+	+	−
M16	38.4	377	214, **164**	+	+	−	+
M17	39.4	393	375, 347, 269, **241**, 198, 125	+	+	+	−
M18	41.6	nd	na	+	+	−	−
M19	46.5	299	271, 257, 215, **198**, 170, 156	+	−	+	−
M20	48.4	439	421, 403, **299**, 215, 198, 141	+	+	+	−
M21	51.8	338	320, 296, **198**, 170, 156	+	+	+	−
M22	53.2	409	338, 269, **241**, 198	+	+	+	−

nd, not determined since a MS signal unique from endogenous ions detected in control incubations was not generated under positive or negative Turbo-ion spray nor positive atmospheric pressure chemical ionization techniques; na, not applicable.

[a] Bold font denotes base peak *m/z* within collision-induced dissociation spectrum.

[b] Compound was (+) or was not (−) detected radiochromatographically within samples from mono-radiolabeled incubations using [^{14}C]**1** or [^{3}H]**1**.

[c] Compound was (+) or was not (−) detected spectroscopically by precursor ion 198 (PC 198) or neutral loss 163 (NL 163) scanning of incubation samples.

60 min of incubation (Table 4), the sum of ^{14}C-only metabolites equaled that of ^{3}H-only metabolites. However, the previously described "cross-talk" concerns of ^{14}C-spillover into the ^{3}H channel was knowingly observed in dual-radiolabel incubations for **2** most notably (i.e. 8% of total ^{3}H within the radioachromatogram) in the in-line ^{3}H-radiochromatogram (Fig. 4), but also to a very minor amount (0.5%) in the LSC-generated radiochromatogram (Fig. 5). Nonetheless, this demonstrated the advantage of simultaneous dual-radiolabel analyses by LSC versus in-line radiodetection.

3.3. Structural rationalization of 1 and its metabolites

The premise behind the need for a dual-radiolabeled substrate proved correct, and the observation of metabolite peaks in respective mono-radiolabel studies using either [^{14}C]**1** or [^{3}H]**1** significantly aided metabolite structure elucidation. Specifically, while detection of a metabolite by ^{14}C-conditions, but not by ^{3}H-conditions, suggested it lacked the fluoropyridine of **1**, the converse meant the metabolite had lost the benzimidazole of **1**. Detection of a metabolite by both ^{14}C- and ^{3}H-conditions suggested it contained both the benzimidazole and fluoropyridine functionalities of **1**. The availability of authentic standards **2** and **3**, as well as both [^{3}H]**1** and [^{14}C]**1**, conveniently provided within each mono-radiolabeled incubation a positive control for the developed analytical methodology for a fully characterized metabolite containing only ^{14}C (i.e. **2** within [^{14}C]**1** incubations), a fully characterized metabolite containing only ^{3}H (i.e. **3** within [^{3}H]**1** incubations), and unchanged **1** containing either ^{3}H or ^{14}C.

Compound **1** had a protonated molecular ion of *m*/*z* 361 and an LC retention time (t_R) of ca. 50.1 min. Because of the characteristic fragment ions contained in the collision-induced dissociation (CID) spectrum of **1** (Fig. 6), two diagnostic MS scans were used with radiochromatographic data as a starting point to elucidate metabolites structurally: precursor ion scan of *m*/*z* 198, corresponding to an unchanged benzimidazole moiety; and, neutral loss of 163 scan, representing loss of an unmodified fluoropyridine imidazole. If compound-related ions, which were determined to be unique from endogenous ions detected in compound-free incubations, were detected by either of these preliminary diagnostic MS/MS scans, then their CID spectra were generated. Proposed metabolite structures were rationalized by a combination of the mono-radiolabel data and comparison of metabolite fragmentation spectra ions to the structure assigned to each fragment within the CID spectrum of **1**. Metabolites, suspected to contain one or more oxygen atoms, were subjected to $TiCl_3$ to determine if they contained an *N*-oxide [20,21]. A summary of all metabolite LC–MS/MS data is found in Table 5, and detailed structural rationalization for each metabolite is summarized in the accompanying supplementary data. The identification of a metabolite as a synthetic standard was determined by the molecules' indistinguishable CID spectra and LC t_R, as well as an increase in metabolite MS peak height following addition of the authentic standard to the analytical sample.

A total of 21 NADPH-dependent metabolites were observed across species (Fig. 7), and all human metabolites were observed in RLMs and/or DLMs. Ten metabolites were tentatively identified while two were unequivocally determined, and consisted of: a variety of oxygenation products with the entire core of **1** intact (**M12**, **M15**, **M16**, **M17** and **M22**), two direct *N*-dealkylation products (**2** and **3**), two amidines (**M9** and **M10**), an oxalimide (**M13**), an anhydride (**M19**) and an amide (**M21**). Nine of the metabolites (**M1**, **M3**–**M8**, **M18** and **M20**) remained unidentified, largely due to the inability to ionize the majority of these compounds in either positive or negative ion mode. Unknown metabolite **M5** was a major product in HLMs, where it constituted 18% of net metabolism of **1**.

3.3.1. Qualitative microsomal assessment of 2 and 3

After conducting all radiolabled studies with **1** and using radiometric and MS data to propose its metabolites, authentic standards **2** and **3**, the direct *N*-dealkylation products of **1**, were incubated in RLMs to determine their metabolic fate. This was important since each compound represented a cleavage product of **1** that contained only one radioisotope. In an attempt to detect and quantify non-radiolabeled metabolites (if any) of **2** and **3**, incubation samples were monitored at an analytical wavelength of 254 and 300 nm, respectively.

Compound **2** was incubated in RLMs to investigate its stability. In all incubations (±NADPH), there was no change in the concentration of **2** over time, suggesting that it was inert to both hepatic microsomal metabolism and chemical degradation. In other words, once formed, **2** does not undergo further microsomal metabolism, and arises solely via C_8 *N*-dealkylation of **1** and, most likely, its core-intact metabolites (e.g. **M9**, **M15**, etc.).

Compound **3** was incubated in RLMs to monitor its stability and to gain potentially structural information for unknowns **M1**, **M3**, **M4** and **M5** that only retained ^{3}H in incubations with [^{14}C/^{3}H]**1**. In all incubations lacking NADPH, the concentration of **3** was unchanged over time, suggesting it underwent neither NADPH-independent metabolism nor chemical decomposition. Following 30 and 60 min incubations in the presence of NADPH, the A_{300} peak area of **3** was ca. 53 and 15% of that observed at 0 min, respectively, and no additional peak(s) appeared in the UV chromatogram. These results suggested that the NADPH-dependent metabolites of **3** did not exhibit even minimal UV absorptivities at 300 nm, which is quite reasonable considering any biotransformation of the imidazole within **3** could significantly alter the UV properties of the original substrate rendering metabolites undetectable at 300 nm. These findings precluded our hope to generate UV-peaks exhibiting the same LC t_R as any of the unidentified ^{3}H-only metabolites (**M1**, **M3**–**M5**) arising from the fluoropyridine imidazole of **1**. To investigate the metabolic fate of **3** further, specific MS^2 experiments were performed in an attempt to elicit MS responses for these A_{300}-non-chromophoric metabolites, including precursor ion scans of *m*/*z* 137, 110 and 96 that were fragment ions observed in the CID spectrum of **3** for which structures could be assigned confidently. However, no molecular ion other than **2** was detected by these MS scans in either positive or negative ion mode; a similar inability to ionize **M1** and **M3**–**M5** was also observed in all radiolabeled incubations

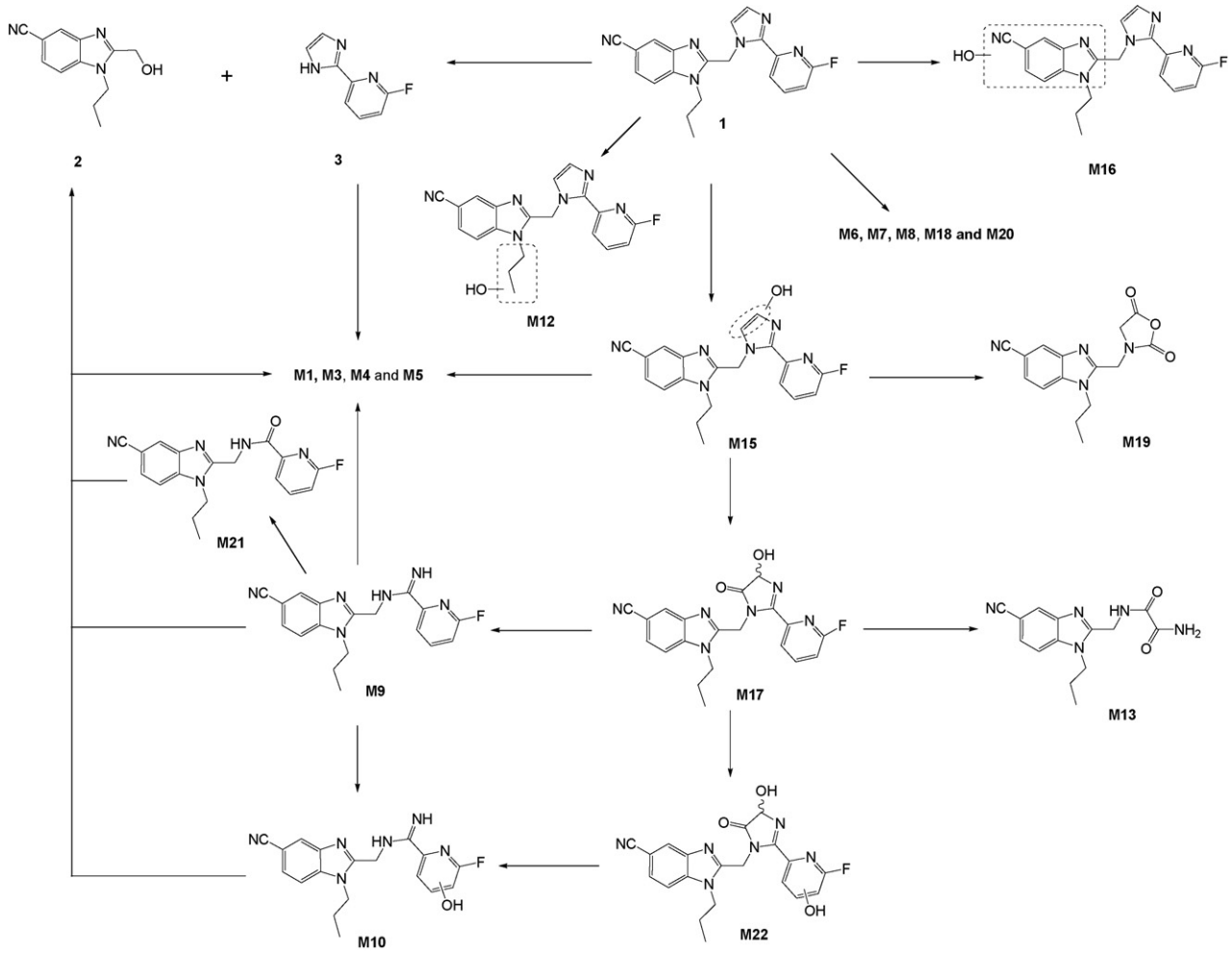

Fig. 7. An overview of the proposed metabolic pathways for **1** in cross-species hepatic microsomes.

(Table 5). In total, these results suggest that **3** is extensively metabolized in a microsomal system containing NADPH, but the identification of its metabolite(s) remains unresolved, leaving undetermined if **M1** and/or **M3**–**M5** arise directly from **3**.

4. Conclusions

The in vitro metabolism of **1** was studied in RLMs, DLMs and HLMs using either [^{14}C]**1**, [^{3}H]**1** or a mixture of both. A schematic overview of the hepatic microsomal metabolism of **1** across species is presented in Fig. 7. Microsomal studies demonstrated unequivocally that the consumption of **1** across species was NADPH-dependent; RLMs metabolized **1** to the greatest extent (>90% after 30 min), followed by DLMs (ca. 49% after 60 min) and HLMs (ca. 42% after 60 min). As species hierarchy increased, so did the number of significant metabolic pathways for **1** in hepatic microsomes. For example, C_8-cleaved metabolites of **1**, which were by far most prominent (ca. 30% of net metabolism) in RLMs, seemed also to be significant (ca. ≥10% of net metabolism) in DLMs and HLMs. However, in the dog and human systems, C_8 *N*-dealkylation was just one of two to four other significant (≥10% of net metabolism) metabolic pathways. In HLMs, the major metabolic pathways appeared to be oxygenation of the fluoropyridine imidazole to afford **M15**, **M17** and **M19**, and C_8-cleaved products **2** and **M5**.

Radiometric analyses of microsomal incubations with [^{14}C]**1** detected metabolites retaining the benzimidazole of **1**. Metabolites **M1**, **3**, **M3**, **M4** and **M5** were not observed radiometrically in these incubations, yet **3**, the only ionizable metabolite of these five, was detected by MS analysis. Alternately, radiometric analysis of microsomal incubations with [^{3}H]**1** detected metabolites maintaining the fluoropyridine, if not the entire fluoropyridine imidazole, of **1**. Metabolites not observed radiometrically in these incubations were **2**, **M13** and **M19**, but all of these ionizable metabolites were detected by MS analysis. As would be predicted, the sum of ^{3}H-only metabolites (i.e. **M1**, **3** and **M3**–**M5**) equaled that of ^{14}C-only metabolites (i.e. **2**, **M13** and **M19**) in all incubations across species, which together allowed the complete elucidation of the metabolic fate of **1**. Mono-radiolabel studies demonstrated that in-line radiometric analysis worked extremely well (and was very reproducible) for quantifying either ^{14}C- or ^{3}H-compounds within *separate* incubations.

When RLMs were incubated with **1** using a mixture of [^{14}C]**1** and [^{3}H]**1**, all metabolites, except **M3**, **M10** and **M13**, previously detected within mono-radiolabeled RLM incubations were observed. Metabolites **M3**, **M10** and **M13**, which are suspected to be downstream secondary or tertiary metabolites, might not have been observed in dual-radiolabeled studies since the average extent of **1** consumption after 60 min (74%) was less than that in mono-radiolabel studies (97%). Nonetheless, these studies demonstrated that the dual-radiolabel strategy provided a comprehensive *qualitative* profile of **1** metabolism. But, the inability of the in-line radiodetector to exclude completely ^{14}C- from ^{3}H-generated counts caused a degree of ambiguity pertaining to metabolite quantification within dual-radiolabel incubations. Thus, to minimize this "cross-talk"-related quantitative uncertainty, which has the potential to inflate artificially ^{3}H-values, LSC analysis of collected dual-radiolabeled incubation LC-fractions was employed to *quantify* both ^{14}C and ^{3}H metabolites simultaneously, while in-line radiodetection was only used for *qualitative* analyses accompanying MS and MS/MS experiments. With this fairly minor and unavoidable, yet readily manageable, caveat of nuclear physics aside, these microsomal analyses demonstrated analytically that dual-radiolabeled **1** could indeed be used for future cross-species in vivo ADME studies.

Acknowledgments

We acknowledge Neurogen Corporation for significant contribution to the collaborative development of **1** with Pfizer Inc., and supplying **1**, **2** and **3**. We also thank Drs. Laura Greenfield and Yinsheng Zhang for the synthesis and purification of [^{14}C]**1** and [^{3}H]**1**, respectively; Messrs. Michael J. Potchoiba and Mark Appel for technical assistance with optimizing radioactive monitors for dual-radiolabel analyses; and, Mr. Mithat Gunduz for conducting lyophilization studies with [^{3}H]**1**.

Appendix A. Supplementary data

Supplementary data associated with this article can be found, in the online version, at doi:10.1016/j.jpba.2006.11.022.

References

[1] D. Dalvie, Curr. Pharm. Des. 6 (2000) 1009–1028.
[2] N.J. Clarke, D. Rindgen, W.A. Korfmacher, K.A. Cox, Anal. Chem. 73 (2001) 430A–439A.
[3] W.A. Korfmacher, M.S. Bryant, K.A. Cox, K. Ng, J. Veals, N.J. Clarke, Y. Hsieh, D. Rindgen, P. Tandler, S. Wainhaus, R.E. White, Adv. Mass Spectrom. 15 (2001) 679–680.
[4] A.P. Watt, R.J. Mortishire-Smith, U. Grhard, T. Thomas, Drug Discov. Dev. 6 (2003) 57–65.
[5] A. Parkinson, in: C.D. Klaassen (Ed.), Casarett and Doul's Toxicology: The Basic Science of Poisons, McGraw-Hill, New York, 2001, pp. 133–224.
[6] T.A. Baillie, M.N. Cayen, H.G. Fouda, R.J. Gerson, J.D. Gree, S.J. Grossman, L.J. Klunk, B. LeBlanc, D.G. Perkins, L.A. Shipley, Toxicol. Appl. Pharmacol. 182 (2002) 188–196.
[7] D.A. Smith, R.S. Obach, Drug Metab. Dispos. 33 (2005) 1409–1417.
[8] R. Kostiainen, T. Kotiaho, T. Kuuranne, S. Auriola, J. Mass Spectrom. 38 (2003) 357–372.
[9] M.R. Anari, T.A. Baillie, Drug Discov. Today 10 (2005) 711–717.
[10] K.A. Cox, in: W.A. Korfmacher (Ed.), Using Mass Spectrometry for Drug Metabolism Studies, CRC Press, New York, 2005, pp. 229–252.
[11] C.E.C.A. Hop, C. Prakash, in: S.K. Chowdhury (Ed.), Identification and Quantification of Drugs, Metabolites and Metabolizing Enzymes by LC–MS, Elsevier, New York, 2005, pp. 123–158.
[12] H.W. Lee, K.J. Won, S.H. Cho, Y.H. Ha, W.S. Park, H.T. Yim, M. Baek, J.H. Rew, S.H. Yoon, S.V. Yim, J.H. Chung, K.T. Lee, J. Chromatogr. B 821 (2005) 215–220.
[13] K.K. Loboz, A.S. Gross, J. Ray, A.J. McLachlan, J. Chromatogr. B 823 (2005) 115–121.
[14] J.H. Woods, G. Winger, Psychopharmacology 118 (1995) 107–115.
[15] A.C. Foster, M.A. Pelleymounter, M.J. Cullen, D. Lewis, M. Joppa, T.K. Chen, H.P. Bozigian, R.S. Gross, K.R. Gogas, J. Pharmacol. Exp. Ther. 311 (2004) 547–559.
[16] B. Drexler, C. Grasshoff, U. Rudolph, K. Unertl, B. Antkowiak, Anaesthesia 55 (2006) 287–295.
[17] B.S. Friesen, Radiation Safety in the Use of Radioactive Materials, University of Kansas, Lawrence, 1996.
[18] L.E. Feinendegen, Tritium-Labeled Molecules in Biology and Medicine, Academic Press, Inc., New York, 1967.
[19] A.C. Veltkamp, H.A. Das, R.W. Frei, U.A.T. Brinkman, Anal. Chim. Acta 233 (1990) 181–189.
[20] P. Kulanthaivel, R.J. Barbuch, R.S. Davidson, P. Yi, G.A. Rener, E.L. Mattiuz, C.E. Hadden, L.A. Goodwiin, W.J. Ehlhardt, Drug Metab. Dispos. 32 (2004) 966–972.
[21] C.L. Shaffer, M. Gunduz, T.N. O'Connell, R.S. Obach, S. Yee, Drug Metab. Dispos. 33 (2005) 1688–1699.